# Thermally evaporated thin film microcrystalline silicon solar cells on polyimide substrate with multiple light trapping schemes

M. Z. PAKHURUDDIN*, K. IBRAHIM, A. ABDUL AZIZ
*Nano-Optoelectronics Research and Technology Laboratory, School of Physics, Universiti Sains Malaysia, 11800 Minden, Penang, Malaysia*

This paper investigates the properties of thermally evaporated p-i-n junction thin film microcrystalline silicon (μc-Si) solar cells on polyimide substrate with multiple light trapping schemes. Hall effect measures doping density of 6.63 x $10^{18}$ $cm^{-3}$ for 500 nm p-type Si and 4.87 x $10^{19}$ $cm^{-3}$ for 120 nm n-type Si produced by co-evaporation of silicon with aluminium and antimony respectively. Raman spectra reveals a peak 511 $cm^{-1}$ with a shoulder at 480 $cm^{-1}$, suggesting microcrystalline nature of the intrinsic 800 nm absorber layer with crystalline volume fraction of ~65%. High resolution X-ray diffraction illustrates that μc-Si grains are in (111) orientation from the peak at 28.9° (orthorhombic crystal structure) and full width at half maximum of 0.2952°. UV-Vis spectrophotometer shows that absorption coefficient of the μc-Si absorber has a gradual increase from 1.1 eV towards higher photon energy with a fairly high absorption (~$10^4$ $cm^{-1}$) in the visible region (1.55 – 3.10 eV). The band gap ($E_g$) of the μc-Si absorber layer is derived to be ~1.2 eV from Tauc plot. The best solar cell records short-circuit current = 8mA, open-circuit voltage = 410 mV and efficiency = 2.0% from current-voltage curve owing to light trapping strategies within the cell.

(Received January 14, 2013; accepted March 13, 2014)

*Keywords:* Thermal evaporation, Polyimide, Thin film microcrystalline silicon solar cells, X-ray diffraction, Light trapping

## 1. Introduction

Polyimide (PI) is an excellent polymeric material. It has attracted interests of many parties in photovoltaic (PV) research and development activities due to its flexibility, light-weight, low-cost, high temperature resistance (typically up to 400°C processing temperature), low coefficient of thermal expansion (CTE), low moisture uptake and also high voltage endurance [1]. Due to its superior properties, PI has found broad applications as substrates in flexible thin film solar cells, flexible printed circuits and high density interconnects [2, 3].

Works of thin film Si solar cells on PI substrate via thermal evaporation technique are hardly reported in the literature. One of the reasons is due to its relatively inferior film quality (e.g. conformality, step coverage and uniformity) produced by highly-directional evaporation process compared to the commonly used chemical vapour deposition (CVD) technique [4]. In this paper, we fabricate thermally evaporated thin film μc-Si solar cells (with p-i-n junction structure) on PI substrate via thermal evaporation technique. Structural, optical, surface morphology and electrical properties of the evaporated cells are investigated. Effects of multiple light trapping schemes towards cells performance are also reported.

## 2. Experimental methods

In this experiment, PI of 75 μm thickness from DuPont Corporation is used as a substrate to fabricate thermally evaporated thin film Si solar cells. Firstly, the substrate is cleaned in Decon 90 chemical for 10 minutes to remove contamination. After the cleaning process, the substrate is rinsed with deionised (DI) water to remove the residue of Decon 90. The substrate is then dipped in isopropyl alcohol (IPA) and agitated with medium ultrasonic power for 10 minutes. Finally, the substrate is dipped in DI water and dried off with nitrogen ($N_2$) gas.

The fabrication of thermally evaporated thin film μc-Si p-i-n junction solar cells on PI substrate is started with 1 μm thickness Al back contact (as positive electrode) deposition via ALCATEL thermal evaporation system at 3.0 x $10^{-5}$ Torr using Al pellets (99.9% purity) as the source material. After the deposition, the contact is annealed at 400°C for 30 min in $N_2$ ambient to ensure good contact properties and improve adhesion to the PI substrate. The p-type Si is also deposited on the same system. Si (99% trace metal basis) and Al powder (99.9% purity) are co-evaporated at 7.5 x $10^{-6}$ Torr to produce 500 nm thickness p-type Si with 5 x $10^{18}$ $cm^{-3}$ doping density. The sample is then annealed at 400°C in $N_2$ ambient for 2 hours to increase crystallinity and improve the distribution of Al atoms in the Si lattice thus ensuring a better doping uniformity across the film. The deposition of the 800 nm intrinsic Si absorber layer is carried out at 7.5 x $10^{-6}$ Torr also on the same system. The n-type Si is deposited on the same system via co-evaporation of Si (99% trace metal basis) and antimony (Sb) powder (99.5% trace metal basis) at 7.5 x $10^{-6}$ Torr to produce 120 nm with around 5 x $10^{19}$ $cm^{-3}$ doping density. To complete the

structure, 1 µm thickness of silver (Ag) contact is deposited to form the front contact (as negative electrode) at 3.0 x $10^{-5}$ Torr using Ag pellets (99.99% purity) as the source material. After the deposition, the sample is annealed in the tube furnace at 400°C for 10 min in $N_2$ ambient to reduce Ag contact resistance and to improve its adhesion to the n-type Si layer.

*Table 1. Samples of thermally evaporated thin film µc-Si solar cells on PI substrate fabricated with multiple light trapping schemes.*

| Cell | Light trapping scheme | | | |
|---|---|---|---|---|
| | Planar | Textured | ZnO (80 nm) | BSR (1 µm) |
| A | X | | | |
| B | | X | | |
| C | | X | X | |
| D | | X | X | X |

In this experiment, 4 samples with different light trapping schemes are prepared as illustrated by Table 1. Cell A is fabricated without any texturing (i.e. planar). Cell B is PI-textured by copper seeding technique [5] before the deposition of Al back contact. Cell C is textured in the same way but deposited with 80 nm ZnO ARC layer, produced via RF-sputtering technique. Cell D is equipped with all the previous light trapping schemes together with a 1 µm white paint back surface reflectance (BSR) layer beneath the cell (by spray technique). The schematic configuration of the cell with full light trapping schemes (as Cell D) is shown in Fig. 1.

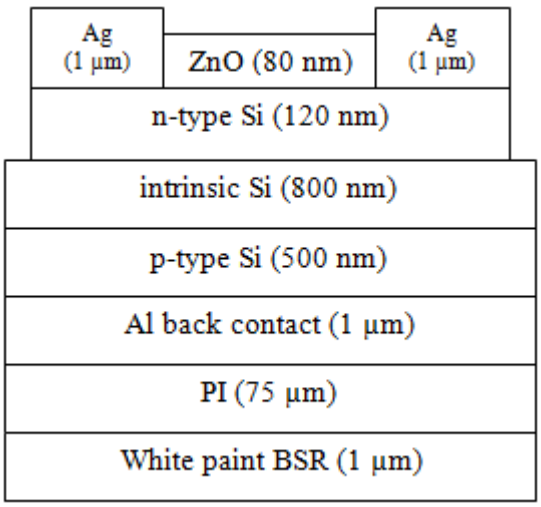


*Fig. 1. Schematic configuration of thermally evaporated thin film µc-Si solar cell on PI substrate (not drawn to scale).*

Thickness of every deposited layer is measured by optical reflectometer (Model: Filmetrics F20) system. Structural properties of intrinsic Si are verified by Raman spectroscopy (Model: Jobin Yvon HR 800 UV) and HR-XRD (Model: PANalytical X'Pert PRO MRD PW3040). Optical properties of intrinsic Si are measured on UV-Vis spectrophotometer (Model: Hitachi U-2000). Electrical properties of the p-type Si and n-type Si layers are measured on Hall effect system (Model: Accent/HL 5500 PC). Current-voltage (I-V) characteristics of the completed cells (Cell A, B, C and D) are measured by the solar simulator system (Model: Solar Simulator 1000 from Optical Radiation Corporation). For this measurement, 4 $cm^2$ cells are placed under 220 $W/m^2$ light intensity (with Xenon Arc lamp) under AM1.5 setting at 25°C. From this measurement, open-circuit voltage ($V_{oc}$), short-circuit current ($I_{sc}$), maximum voltage ($V_{max}$), maximum current ($I_{max}$), fill factor (F.F) and efficiency (η) of the solar cells are extracted and analyzed.

## 3. Results and discussion

Hall effect system measures doping density of $6.63 \times 10^{18}$ $cm^{-3}$ for the 500 nm p-type Si and $4.87 \times 10^{19}$ $cm^{-3}$ for the 120 nm n-type Si. The results show heavy doping levels of both sides of the cell that could help establish a strong electric field across the intrinsic Si absorber layer which in turn improves carrier collection efficiency [6].

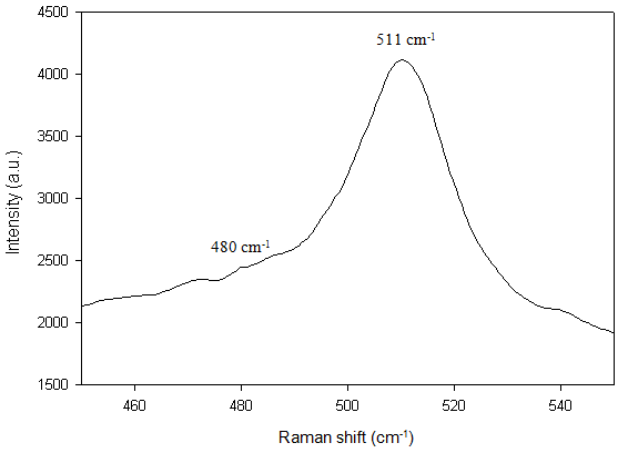


*Fig. 2. Raman spectra of 800 nm intrinsic Si absorber layer.*

Fig. 2 shows the Raman spectra of 800 nm intrinsic Si absorber layer evaporated on p-type Si/Al/PI stack. From the spectra, it can be observed that a crystalline Si peak emerges at 511 $cm^{-1}$ with FWHM of 19 $cm^{-1}$. Besides, a very low amorphous Si (a-Si) shoulder is also evident at 480 $cm^{-1}$, indicating that this layer is microcrystalline (µc-Si) in nature; with presence of crystalline phases within amorphous matrix. The microcrystalline nature of

the sample is believed to be due to the annealing of the p-type Si (previous layer) that provides seeding effect for the crystalline grains to grow [7]. The crystalline volume fraction ($X_c$) of the sample is calculated by using the following equation [8]:

$$X_c = I_c/(I_c + mI_a)\ \% \quad (1)$$

where;
$X_c$ = crystalline volume fraction (%)
$I_c$ = deconvoluted intensity of crystalline peak (a.u.)
$I_a$ = deconvoluted intensity of amorphous peak (a.u.)
m = constant

By using the above equation, the $X_c$ is calculated to be around 65%. The result indicates the presence of significant fraction of amorphous regions in the film, which could be attributed to high density of dangling bonds. The dangling bonds are typically deep amphoteric defect states located in the mid-gap of the Si material and are effective carrier recombination centres [9].

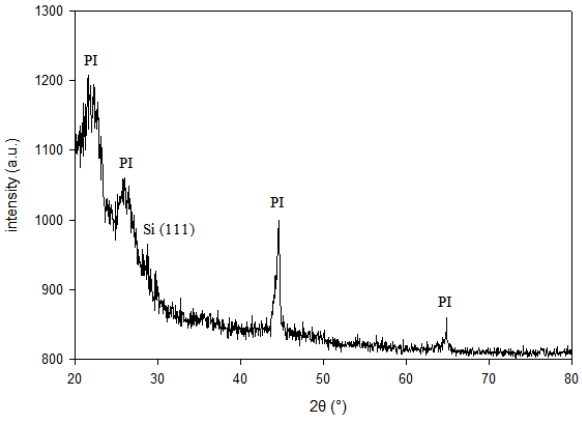


*Fig. 3. HR-XRD pattern of 800 nm intrinsic µc-Si absorber layer.*

Fig. 3 plots the HR-XRD pattern of 800 nm intrinsic µc-Si absorber layer evaporated on p-type Si/Al/PI stack measured between 20° - 80° (2Θ). The output pattern is compared to International Centre for Diffraction Data (ICDD) library [10]. The sample shows a low peak of Si (111) at 28.9° (orthorhombic crystal structure) with FWHM of 0.2952°. The diffraction from the Si (111) plane explains the presence of crystalline Si peak in the previous Raman spectra at 511 $cm^{-1}$. Another 4 peaks in the diffraction pattern at 22.1°, 25.9°, 44.6° and 64.9° belong to PI substrate [11].

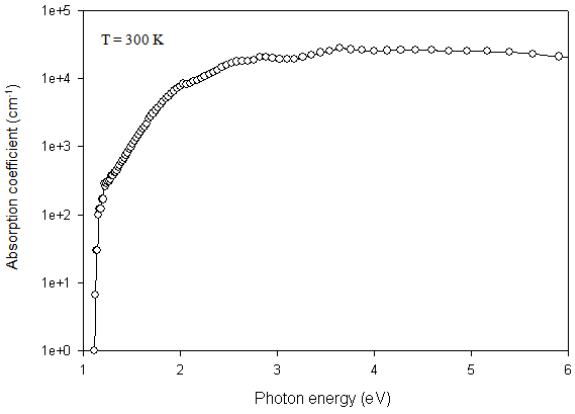


*Fig. 4. Absorption coefficient of 800 nm intrinsic µc-Si absorber layer.*

Fig. 4 illustrates the logarithmic plot of absorption coefficient (α) of 800 nm intrinsic µc-Si absorber layer evaporated on p-type Si/Al/PI stack measured at 300 K across the photon energy of 1 – 6 eV (corresponding to 200 – 1100 nm). For this measurement, the p-type Si/Al/PI sample is placed in the reference compartment to exclude the effects of previous layers on the value of absorption coefficient of the intrinsic Si layer. From this figure, it can be seen that the absorption coefficient of the µc-Si shows a gradual increase (from zero) at 1.1 eV towards higher photon energy. Apart from that, a fairly high absorption in the visible region (1.55 – 3.10 eV) could be attributed to the absorption of the a-Si phase within the film. From the curve, it can be concluded that the µc-Si film can be used as an absorber layer in the fabricated solar cells.

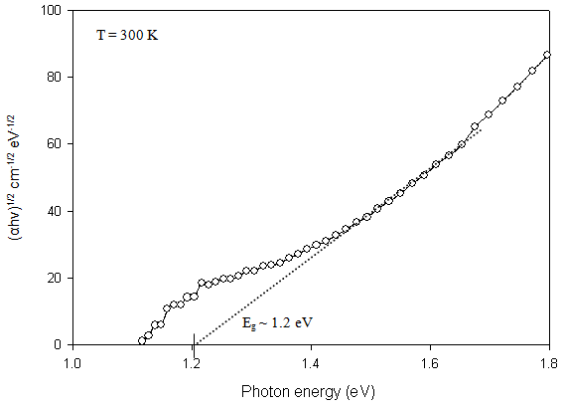


*Fig. 5. Plot of $(\alpha h\nu)^{1/2}$ as a function of photon energy (hν) of intrinsic µc-Si absorber layer.*

Fig. 5 is derived from the absorption coefficient data in Fig. 4. For an indirect band gap material like Si, relationship between the absorption coefficient (α) and the band gap ($E_g$) is given by Tauc equation [12] as the following:

$$(\alpha h\nu)^n = B(h\nu - E_g) \quad (2)$$

where;
$\alpha$ = absorption coefficient ($cm^{-1}$)
hv = photon energy (eV)
n = ½ (implies indirect optical transition in Si)
B = constant
$E_g$ = optical band gap of the film (eV)

From the above relationship, $(\alpha h\nu)^{1/2}$ is plotted as a function of photon energy (hv) of the intrinsic µc-Si absorber layer. Then, the optical band gap ($E_g$) of the film is estimated by extrapolating the linear part of the curve to an interception at the x-axis where the $(\alpha h\nu)^{1/2} = 0$. From the linear extrapolation (as shown by the above figure), the optical band gap ($E_g$) of the µc-Si absorber is determined to be ~1.2 eV. The value confirms the microcrystalline nature of the film which normally has a band gap of around 1.1 eV [13]. The slightly higher $E_g$ obtained from this curve could possibly be attributed to the defects introduced within the film during the deposition process [4]. The result shows a good agreement with the result demonstrated by the Raman spectra in Fig. 2.

*Table 2. Summary of I-V curve of thin film µc-Si solar cells (p-i-n junction) on PI substrate with multiple light trapping schemes. The cells were tested using solar simulator system under 220 W/m$^2$ illumination under AM1.5 at 25°C (Cells area = 4 cm$^2$).*

| Cell | Isc (mA) | Voc (mV) | Imax (mA) | Vmax (mV) | F.F (%) | η (%) |
|---|---|---|---|---|---|---|
| A | 3.8 | 370 | 3.0 | 240 | 51.9 | 0.8 |
| B | 6.1 | 372 | 4.4 | 260 | 50.7 | 1.3 |
| C | 7.1 | 390 | 4.9 | 300 | 52.3 | 1.7 |
| D | 8.0 | 410 | 5.9 | 300 | 53.5 | 2.0 |

Table 2 summarizes the $I_{sc}$, $I_{max}$, $V_{oc}$, $V_{max}$, F.F and η of thin film µc-Si solar cells (p-i-n junction) on PI substrate with multiple light trapping schemes tested using Solar Simulator 1000 from Optical Radiation Corporation. The tests are carried out under 220 W/m$^2$ light illumination at AM1.5 condition with temperature of 25°C. The area of the cells is 2 × 2 cm$^2$ (i.e. 4 cm$^2$). The I-V curve is plotted in Fig. 6 for further clarity.

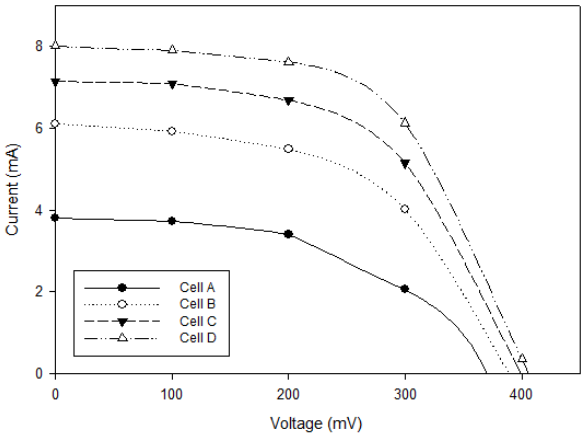


*Fig. 6. I-V characteristics of illuminated (AM 1.5, 220 W/m$^2$, 25°C) thin film µc-Si solar cells (p-i-n junction) on PI substrate with multiple light trapping schemes.*

Fig. 6 plots the illuminated I-V characteristics of thin film µc-Si solar cells (p-i-n junction) on PI substrate with multiple light trapping schemes. From the curves, it can be seen that Cell A (with planar structure) records the lowest $I_{sc}$; 3.8 mA owing to lack of light trapping within the cell. $V_{oc}$ measures only 370 mV indicating a poor p-i-n junction quality that could also be due to significant carrier recombination at the junction region besides possible formation of shunting path within the cell [14]. Fill factor and efficiency of this cell are 51.9% and 0.8% respectively.

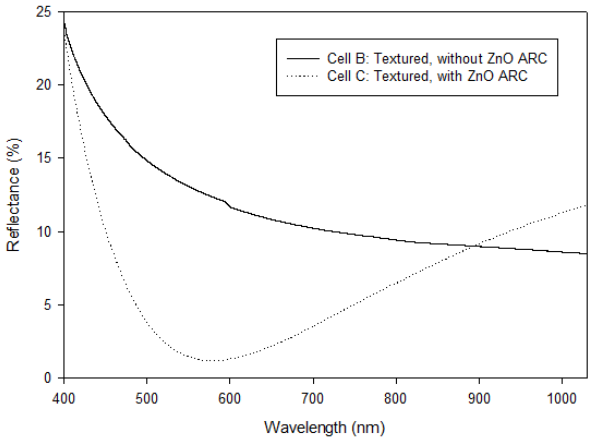


*Fig. 7. Front surface reflectance plots between cells with and without ZnO ARC.*

Cell B (with surface texturing) shows an increase in $I_{sc}$ to 6.11 mA due to improved light trapping effect within the cell while the surface reflection loss has been suppressed to only around 10% (as shown in Fig. 7). Fill factor measures 50.7% and efficiency increases to 1.3%. Cell C (with the 80 nm ZnO ARC layer) illustrates a 17% increase in the value of $I_{sc}$ (to 7.14 mA) due to suppression of the red region (~600 nm) of solar spectrum by quarter-wavelength (λ/4) ARC coating (also shown by Fig. 7). $V_{oc}$ also records a slight increase with the improvement in light trapping scheme. This cell measures 1.7% efficiency with 52.3% fill factor.

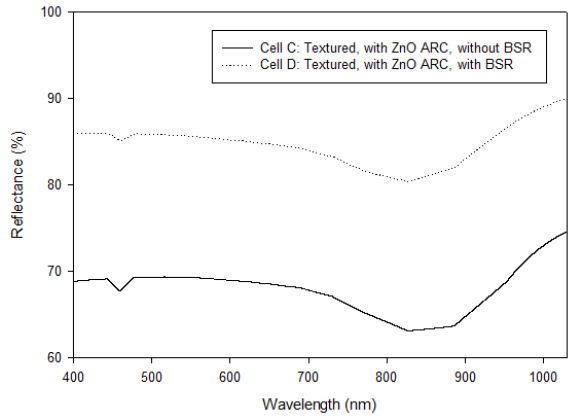


*Fig. 8. Rear surface reflectance plots between cells with and without white paint BSR.*

The best result is achieved from Cell D (textured, 80 nm ZnO ARC and 1 µm white paint BSR layer). On this cell, 8 mA of $I_{sc}$ and 410 mV of $V_{oc}$ with fill factor of 53.5% and efficiency of 2.0% are recorded from the measurement. About 12% and 6.5% respective increase in the $I_{sc}$ and $V_{oc}$ are measured in comparison to Cell C after the incorporation of the cheap white paint BSR at the rear of the cell that boosts the light trapping efficiency by increasing rear surface reflectance (shown in Fig. 8) [15]. From the figure, it can be seen that the rear surface reflectance increases about 17% (average in the visible region); from around 68% to 85% after the incorporation of the white paint BSR. This implies that the incorporation of the highly reflective BSR is very important in compensating the moderate reflectance values of the textured Al back contact recorded earlier.

Efforts are underway to increase the efficiency of the cells produced via thermal evaporation technique. These include optimisation of absorber thickness, p-type and n-type thicknesses and doping levels and also optimisation of Al rear contact thickness and contact area to reduce possibility of shunting the cells. Besides, optimisation of white paint BSR is also in progress in order to boost optical absorption from low energy photons via their "second-pass" through the absorber layer.

## 4. Conclusions

In this paper, the properties of thermally evaporated p-i-n junction thin film µc-Si solar cells on PI substrate with multiple light trapping schemes are studied. Hall effect records $6.63 \times 10^{18}$ $cm^{-3}$ and $4.87 \times 10^{19}$ $cm^{-3}$ doping density for 500 nm p-type Si (Al-doped) and 120 nm n-type Si (Sb-doped) respectively. Raman spectra reveals a peak 511 $cm^{-1}$ with a shoulder at 480 $cm^{-1}$, suggesting microcrystalline nature of the 800 nm absorber layer with $X_c$ ~65%. HR-XRD illustrates that µc-Si grains are in (111) orientation (peak at 28.9°, FWHM of 0.2952°). UV-Vis spectrophotometer shows that absorption coefficient of the µc-Si absorber layer has a gradual increase at 1.1 eV towards higher photon energy with a fairly high absorption (~$10^4$ $cm^{-1}$) in the visible region (1.55 – 3.10 eV). From Tauc plot, the $E_g$ of the µc-Si absorber is derived to be ~1.2 eV. The best solar cell records $I_{sc}$ = 8mA, $V_{oc}$ = 410 mV and $\eta$ = 2.0% after improvement in light trapping.

**Acknowledgements**

The support of Universiti Sains Malaysia and financial assistance from Incentive Grant 1001/ PFIZIK/821061 is gratefully acknowledged. Thanks to DuPont Corporation (Malaysia and Singapore) for contributing the PI samples for this work.

## References

[1] DuPont. (2012, 11 May). Kapton® polyimide film. Available: http://www2.dupont.com/Kapton/en_US/index.html.
[2] X. -T. Hao, J. Ma, D. -H. Zhang, Y. -G. Yang, H. -L. Ma, C. -F. Cheng, X. –D. Liu, Materials Science and Engineering: B **90**, 50 (2002).
[3] H. Gleskova, S. Wagner, Electron Device Letters **20**, 473 (1999).
[4] S. Klein, T. Repmann, T. Brammer, Solar Energy **77**, 893 (2004).
[5] N. L. D. Somasiri, T. A. Speckhard, Polyimide substrate having a textured surface and metallizing such a substrate, USA Patent **4**, 975, 327 (1990).
[6] M. A. Green, Silicon Solar Cells: Advanced Principles & Practice, Sydney: Centre for Photovoltaic Devices and Systems University of New South Wales, (1995).
[7] G. Beaucarne, F. Duerinckx, I. Kuzma, K. V. Nieuwenhuysen, H. J. Kim, J. Poortmans, Thin Solid Films **511**, 533 (2006).
[8] R. E. I. Schropp, M. Zeman, Materials and Device Technology, Kluwer Academic Publishers, (1998).
[9] J. Nelson, The Physics of Solar Cells, Imperial College Press, (2003).
[10] ICDD. (2012, 10 July). International Centre for Diffraction Data (ICDD). Available: http://www.icdd.com/
[11] M. Z. Pakhuruddin, K. Ibrahim, A. Abdul Aziz, Advanced Materials Research **620**, 474 (2013).
[12] G. P. Smestad, Optoelectronics of Solar Cells, SPIE Press, (2002).
[13] M. F. Cerqueira, J. A. Ferreira, G. J. Adriaenssens, Thin Solid Films **370**, 128 (2000).
[14] M. A. Green, Solar Cells: Operating Principles, Technology, and System Applications, Prentice-Hall, (1982).
[15] O. Berger, D. Inns, A. G. Aberle, Solar Energy Materials and Solar Cells **91**, 1215 (2007).

*Corresponding author: zamirlitho@gmail.com